Coherent supercontinuum generation in all-normal dispersion Si<inf>3</inf>N<inf>4</inf> waveguides

Coherent supercontinuum generation in all-normal dispersion Si_3N_4 waveguides

ISRAEL REBOLLEDO-SALGADO,[1,2,*] ZHICHAO YE,[1] SIMON CHRISTENSEN,[3] FUCHUAN LEI,[1] KRISHNA TWAYANA,[1] JOCHEN SCHRÖDER, [1] MARTIN ZELAN,[2] AND VICTOR TORRES-COMPANY[1]

[1]*Department of Microtechnology and Nanoscience (MC2), Photonics Laboratory Chalmers University of Technology, SE-41296, Sweden*
[2]*Measurement Science and Technology, RISE Research Institutes of Sweden, SE-501 15 Borås, Sweden*
[3]*Photonics Department, Technical University of Denmark, 2800 Kgs. Lyngby, Denmark*
[*]*israels@chalmers.se*

Abstract: Spectral broadening of optical frequency combs with high repetition rate is of significant interest in optical communications, radio-frequency photonics and spectroscopy. Silicon nitride waveguides (Si_3N_4) in the anomalous dispersion region have shown efficient supercontinuum generation spanning an octave-bandwidth. However, the broadening mechanism in this regime is usually attained with femtosecond pulses in order to maintain the coherence. Supercontinuum generation in the normal dispersion regime is more prone to longer (ps) pulses, but the implementation in normal dispersion silicon nitride waveguides is challenging as it posses strong requirements in propagation length and losses. Here, we experimentally demonstrate the use of a Si_3N_4 waveguide to perform coherent spectral broadening using pulses in the picosecond regime with high repetition rate. Moreover, our work explores the formation of optical wave breaking using a higher energy pulse which enables the generation of a coherent octave spanning spectrum. These results offer a new prospect for coherent broadening using long duration pulses and replacing bulky optical components.

1. Introduction

Broad bandwidth frequency combs with high repetition rate have found a myriad of applications in fields such as optical communications [1, 2], radio-frequency (RF) photonics [3, 4] and spectroscopy [5, 6]. Spectral broadening of high repetition rate frequency combs can be done by supercontinuum generation [7]. Earlier works focused on silica-based nonlinear fibers as the nonlinear platform, but in the past few years alternative planar integrated waveguide technologies have emerged, like silicon [8, 9], silicon nitride (Si_3N_4) [10, 11], AlGaAs [12] or lithium niobate [13].

The supercontinuum (SC) generation in Si_3N_4 has attracted significant interest since it offers a high nonlinear coefficient and a wide transparency range without two-photon absorption in the near infrared [14]. In this platform, more studies have reported octave-spanning SC spectrum by exploiting the dispersion engineering capabilities and low losses attainable in Si_3N_4 waveguides [10, 11, 15, 16]. These previous works have focused in the anomalous dispersion regime in combination with femtosecond pulses, where the coherence is maintained with relatively short propagation lengths and low energy pulses [17]. When pumping the waveguide in the anomalous dispersion region, the major broadening mechanisms are soliton compression and the generation of dispersive waves [18]. When pumping with longer (ps) pulses, the soliton self-compression effect can be utilized [19] to attain coherent broadening. This strategy has been recently implemented in silicon nitride waveguides [20].

A well known alternative for the generation of coherent spectra using picosecond pulses as pump source is using a high non-linear fiber (HNLF) working in the normal dispersion

regime [21–25]. In this approach, the SC generation benefits of the typical low-losses and long lengths of optical fibers, nevertheless, obtaining similar results on integrated waveguides poses a challenge. Ultralow-losses in micro-ring resonators have been reported in Si_3N_4, but attaining low-losses in dispersion-engineered, high-confinement waveguides have only been achieved recently [26–28]. The SC generation on chip in the all-normal dispersion (ANDi) regime has been reported in silicon-rich silicon nitride waveguides [29] and by engineering the dispersion of the polarization modes in Si_3N_4 [30]. The dominant nonlinear processes in the ANDi region are self-phase modulation (SPM) and optical wave breaking (OWB) [31], hence the bandwidth of the SC is reduced in comparison with the anomalous dispersion case [11, 18]. However, SC generation in ANDi waveguides does not exhibit fine spectral structure neither large dips since it does not rely on soliton processes or dispersive wave generation. By suppressing all soliton dynamics, the amplification of input shot noise inherent to modulation instability (MI) is avoided and the coherence of the spectra is preserved [32] when pumping with picosecond pulses. The duration of the seed pulse to perform coherent broadening in the ANDi regime is limited by Raman-amplified noise and polarization MI [33].

In this work, the generation of SC in the ANDi region is reported using a long Si_3N_4 waveguide with ultra-low loss and engineered with low and flat group velocity dispersion (GVD). By using a Gaussian shaped picosecond pulse as a pump, we broadened its initial bandwidth up to 2.5 times achieving a flat and stable spectrum. To the best of our knowledge, we report for the first time an octave broadening in an ANDi Si_3N_4 integrated waveguide pumping with a femtosecond pulse. We demonstrate the high quality of the noise and stability of the generated spectra for both pumping schemes. These results highlight the potential of silicon nitride waveguides as an alternative to optical fibers in the normal dispersion region for SC generation. The robustness in terms of flatness and noise performance of the SC generated in the ANDi waveguide makes it an ideal source for applications such as pulse compression into the few cycle regime, self-referencing of high repetition rate frequency combs, optical coherence tomography and telecommunications. Combined with the possibility to engineer the dispersion profile in the near infrared and visible ranges, this work also opens an avenue of opportunities for the realization of astronomical spectrographs [34] and the generation of comb light sources for biomedical imaging [5].

2. ANDi silicon nitride waveguide

The waveguide is fabricated in Si_3N_4 using a subtractive processing method [35]. The waveguide consists of three cascaded Archimedean-spirals to attain a length of 20 cm within a device footprint of 3 mm^2. A microscopic image of a single spiral waveguide unit is shown in Fig. 1 (a). The waveguide with a core geometry of 2700 x 690 nm^2 was simulated in the finite element method solver COMSOL Multiphysics using the refractive index data of the silicon nitride and silica cladding materials. The waveguide sustains up to eight modes.

To reduce the coupling between different transverse modes, an optimized S-bend design was used to connect clock- and anticlock-wise waveguides, and stitching error compensation was introduced between adjacent spiral waveguide units [36, 37]. The GVD profile of the TE mode is shown in Fig. 1(b) and exhibits a low and flat dispersion near the central wavelength of 1550 nm. At this wavelength, the simulated GVD is 15 ps^2/km and the nonlinear coefficient (γ) is 0.7 $(W \cdot m)^{-1}$ for the fundamental TE mode. The nonlinear Kerr coefficient n_2 considered for silicon nitride is $2.4x10^{-19}$ m^2/W [38]. The GVD and the propagation loss of the fabricated spiral waveguide were characterized using a novel OFDR technique where a swept wavelength laser is calibrated against a self-referenced frequency comb [39]. The interference between the reference signal and the reflected signal from the facets is recorded and processed offline. The measured β_2 is equal to 44 ps^2/km at the central wavelength, which is 30 ps^2/km higher than the obtained in the finite-element simulations. This discrepancy can be attributed to the variations in the waveguide geometry and the material refractive index. The thickness of waveguide across the

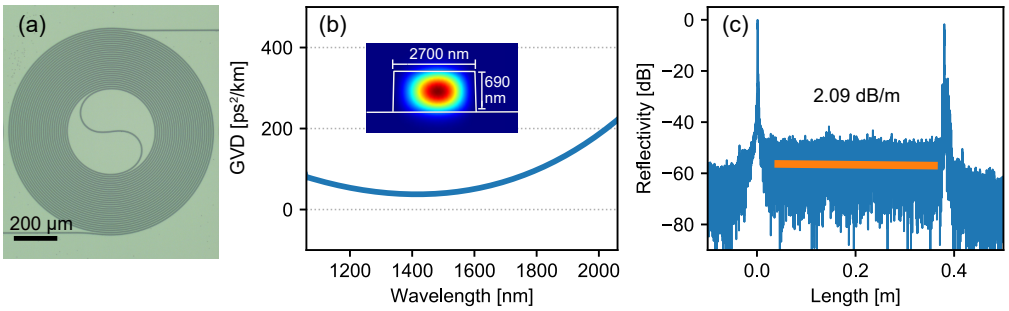

Fig. 1. Silicon nitride waveguide characteristics. (a) Microscopic image of an individual spiral waveguide. (b) Simulated group velocity dispersion (GVD) of the waveguide with a geometry of 2700 nm x 690 nm (Inset) Simulated TE mode profile. (c) Propagation loss measured using an OFDR technique.

wafer varies around 2% due to the silicon nitride deposition process. The width of the fabricated waveguide also shows a deviation with respect to the geometry designed. Small variations in the measurement of the refractive index of the materials can also cause an up/downshifting of the waveguide dispersion [40]. The spatial reflectivity profile shown in Fig. 1(c) is obtained after the post processing of the measurement. The two peaks represent the reflection of the input and output facets and no sharp defects are found along the device. By estimating the gradient of the distributed back-scattering the measured propagation loss is 2.09 dB/m.

3. Spectral broadening of high repetition pulses

In this section, the results obtained when pumping the ANDi waveguide using picosecond pulses are discussed. Electro-optic (EO) frequency combs are of significant interest for its use as seed pulses due to their robustness in terms of power stability and flexibility for tuning the central wavelength [41, 42]. We use an EO-comb in a cascade configuration of four phase modulators (PM) and one intensity modulator in order to extend the bandwidth of the seed pulse. All modulators are driven by a low phase noise RF oscillator with a frequency of 25.1 GHz in a similar arrangement as in [43]. This configuration of the EO-comb yields a flat optical spectrum, therefore a sinc-like pulse is obtained in the temporal domain after compensating the inherent dispersion of the comb. Previous works [7, 44] showed the generation of flat SC spectrum using a directly synthesized Gaussian-shaped electro-optic combs in combination with normal dispersion fibers. Here, to achieve Gaussian shaped pulses, an amplitude apodization of the pulses is implemented [45]. The experimental setup of the nonlinear broadening of the EO-comb pulses using the ANDi waveguide is depicted in the Fig. 2 (a). The shaping of the pulse is performed in a two-step process, first by correcting the linear dispersion and secondly by apodizing the spectral envelope of the comb. The apodizing process allows to obtain a Gaussian shape and correct spectral variations produced by nonlinearities along the optical path. The first step is implemented after the initial EO-comb with a flat spectrum is pre-amplified using a low noise erbium-doped fiber amplifier (EDFA). The autocorrelation trace is measured at the output of the pre-amplifier and optimized in an iterative manner by applying phase filters using a pulse shaper to correct the dispersion [46]. We calculate the transformed limited pulse of the measured optical spectrum. Thereafter, the theoretical intensity autocorrelation of the bandwidth limited pulse is calculated. This simulated auto-correlation trace is used as a reference for the dispersion correction. Although the dispersion of the comb is mainly quadratic, the correction was performed up to the 6th order which allows a near bandwidth-limit compression [41].

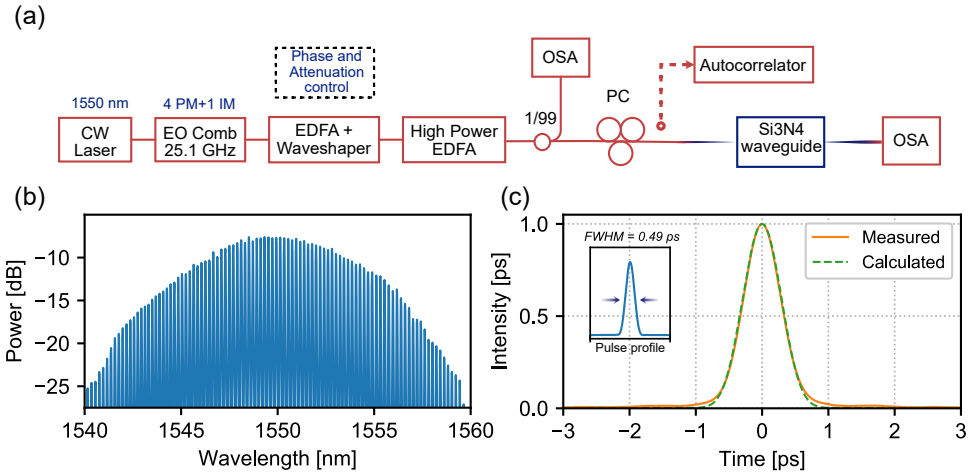

Fig. 2. Pulse compression and supercontinuum generation in an ANDi silicon nitride waveguide.. (a) Diagram of the experimental setup. CW: continuous wave, PM: phase modulator, IM: intensity modulator, EDFA: Er-doped fiber amplifier, PC: polarization controller, OSA: optical spectrum analyzer. (b) Optical spectrum of the Gaussian shaped pump pulse. (c) Normalized intensity auto-correlation of the pump pulse, measured (solid orange) and calculated from spectrum (green dashed). (Inset) Calculated intensity for the transform-limited pulse.

The zero-dispersed pulses pass through a high-power EDFA, since the linear dispersion has been compensated, the peak power of the pulse is high enough to produce non-linear broadening in combination with the fibers of the system. This is corrected in the second step of the shaping, where an iterative Gaussian apodization is implemented by applying amplitude filters in order to obtain a smooth and symmetric spectrum [45]. The optical spectrum of the input pulse is monitored after the high power EDFA with the aid of a 20 dB coupler. The attenuation filters are calculated based on the difference between the target Gaussian shape and the monitored power in an iterative loop. Figure 2 (b) shows the spectrum of the final Gaussian shaped pulse after three iterations, which exhibits approximately 90 lines centered at 1550 nm.

To verify the quality of the compression to its bandwidth limit after the shaping, the intensity autocorrelation of the Gaussian shaped pulse was measured and simulated similarly to the first step. The auto-correlation trace is measured prior to the coupling to the waveguide using a fiber patchcord with the same length as the lensed fiber. The autocorrelation traces measured and simulated are shown in Figure 2 (c). The good agreement between both traces indicates a high quality of compression and high-degree of stability of the input pulse. This allows us to assume a Gaussian profile for the pulse being coupled to the waveguide, with a full width at half maximum of 0.5 ps, inferred from the transform-limited duration. This pulse is used for the numerical simulations of the field propagation in the waveguide.

3.1. Spectral evolution of the picosecond pulse

The picosecond pulse is coupled to the Si_3N_4 waveguide by means of a lensed fiber, the measured coupling losses are 3 dB per facet. The average power coupled at the input is 28.5 dBm. This estimation is made after considering the coupling and the propagation losses. Since the pulse is estimated to have a width of 0.5 ps, a peak power of 62 W at the start of the propagation is considered. The spectral output of the waveguide is recorded with the optical spectrum analyzer. The broadened frequency comb extends from 1525 nm to 1575 nm within the 10 dB bandwidth,

this is 2.5 times the bandwidth of the initial Gaussian spectrum. We performed numerical simulations to contrast the experimental results. The spectral evolution of the pulse propagating in the ANDi waveguide was simulated with the generalized nonlinear Schrodinger equation [47,48]. The simulation considers the measured GVD and the simulated nonlinear parameter (γ) at 1550 nm. The simulated output of the waveguide after a propagation of 20 cm (see Fig.3 (a)) is in excellent agreement with the experimental result shown in Figure 3 (b). In both cases, the central region shows the more significant variations that are result of slight imperfections of the shape of the input pulse. Figure 3 (c) shows the spectral evolution of the pulse while it propagates, the initial spectral variations are maintained along the waveguide. It is clear that the spectral broadening achieved is dominated by SPM since the peak power is not sufficiently high to induce OWB. As a consequence, the spectral envelope does not resemble a rectangular profile with shoulders at the edges. Notwithstanding, the Gaussian shaping applied to the pump pulse helps to minimize the sharp spectral interference. To get a better insight of the spectral evolution of the pulse, a sweep of the input average power was performed. This step was done experimentally and supported by simulations where the same pump pulse was considered at different power levels in a range from 18 to 28.5 dBm. Figure 3 (d) shows the simulated spectrum output of the waveguide as a function of the input average power. The experimental results from sweeping the in-coupled power (shown in Figure 3 (e)) closely resemble the numerical simulation. One can conclude that similar to previous works [7,31,44] the pump pulse characteristics play a major role in the flatness of the broadened spectrum when working in the normal dispersion. In order to access the OWB regime, a longer propagation distance and a higher peak power is needed, which would enhance the broadening.

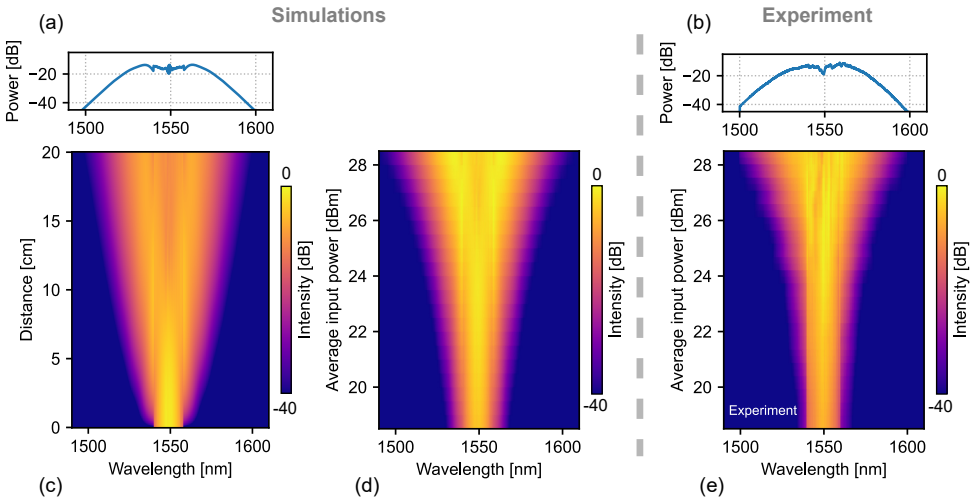

Fig. 3. Nonlinear broadening of EO-combs in an ANDi Si_3N_4 waveguide. (a) Simulated output after 20 cm of propagation. (b) Experimental output of the 20 cm long waveguide (c) Spectral evolution of the pump pulse along the propagation. (d) Simulated output spectra for different average in-coupled power. (e) Measurement of the output spectrum sweeping the in-coupled power.

3.2. Noise and stability of the spectrum

To assess the quality of the broadened spectrum, we characterized the phase noise of the repetition rate and the optical linewidth of the individual lines. We analyzed the single side band (SSB) phase noise of the photo-detected repetition rate of the input Gaussian-shaped and the output broadened spectrum. These measurements were performed using a high-bandwidth photodetector

and the phase-noise function of the electric signal analyzer (ESA). The phase noise of the 25.1 GHz RF clock was directly measured in the ESA for comparison. Figure 4 (a) shows the results of the three SSB phase noise measurements, all the traces are in excellent agreement along the offset frequencies. The inset shows the direct photo-detected beat note of the repetition rate of the EO Comb. Based on this radio-frequency analysis, we conclude that the nonlinear broadening does not appreciably degrade the timing jitter of the comb, similar to results demonstrated in normal dispersion fibers [22].

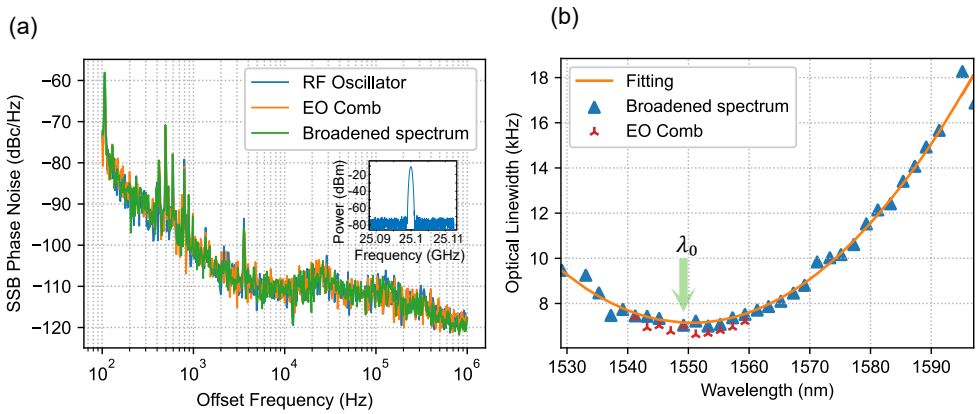

Fig. 4. (a) Measurements of the repetition rate single side band (SSB) phase noise of the RF oscillator (blue), input EO-comb (orange) and broadened spectrum (green), Inset: Photo-detected beat note of the EO comb (b) Optical linewidth of the individual comb lines of the SC generated.

In an optical frequency comb, the optical linewidth will increase as it moves away from the carrier due to the timming jitter. In an electro-optic comb, the timing jitter is given by the finite linewidth of the RF oscillator [49, 50]. A quadratic behavior is then predicted in the phase noise variance when the mode moves away from the center frequency. The phase-error variance can be used to estimate the 3 dB optical linewidth when a Lorentzian line shape is assumed [51]. The optical linewidth of individual lines filtered from the broadened spectrum was studied using a self-heterodyne measurement technique in combination with a coherent receiver [51]. In Figure 4 (b) the measured fundamental linewidths for individual modes are displayed. These values are obtained based on the average value at high offset frequencies within a few MHz span [52, 53]. The result follows the expected parabolic distribution where the lowest linewidth of the SC is located at the pump. From these results, we can deduce a good stability of the SC spectrum over its full bandwidth. The phase-noise characteristics do not show additional degradation due to the chromatic dispersion or nonlinear broadening when photo-detecting the initial EO-comb and the ANDi SC, respectively.

4. Octave spanning broadening using femtosecond pulses

Next, we study the case of SC generation when a femtosecond pulse with a lower repetition rate is used as a pump. Figure 5 (a) shows the experimental setup for the generation of the SC and its coherence study. The seed source is a self-referenced fiber mode-locked frequency comb with a center wavelength of 1560 nm and a repetition rate frequency of 250 MHz. The output pulse has a duration of around 50 femtoseconds which is free space coupled to a waveguide with the same characteristics previously described but without a tapered section. The beam is collimated and expanded before reaching the in-coupling lens to have a diffraction-limited spot size. The

coupling loss at the input facet is estimated to be 8 dB. The higher coupling losses could be a consequence of a sub-optimized overlap of the waveguide mode and the beam profile. The coupling losses are measured at the central wavelength and at low input power to prevent the broadening. In this case, we are also interested in pumping the TE mode where the dispersion is shown to be all-normal. We aligned the polarization state of input pulse while monitoring the power using a half-lambda waveplate with the aid of a linear polarizer. The output is collected using a short-lensed fiber using two different optical spectrum analyzers, one covering from 600 to 1700 nm and other that covers from 1.2 μm to 2.4 μm. Using a femtosecond pulse with an estimated energy of 328 pJ on chip, the generated spectrum in the Si_3N_4 waveguide spans from 1010 nm to 2020 nm with intensity variations within 20 dB. To the best of our knowledge, this is the first time that an octave broadening is obtained in an ANDi Si_3N_4 integrated waveguide.

The SC generated was simulated considering the wavelength dependence of the effective area and nonlinear Kerr parameter and the frequency dependent GVD of the TE mode [54]. The pulse considered for the simulations corresponds to the Fourier-transform limit obtained from the MLL spectrum and measured using an autocorrelator. Both, the experimental and estimated pulse traces show a complex structure that can be attributed to non-linearities in the laser system due the high peak power. To assess the coherence of the SC spectrum generated, we simulated the first order spectral coherence function $g_{12}(\omega)$ for a set of 100 simulated spectra obtained in the GNLSE simulations [55]. In the simulation, quantum noise is added in the initial conditions. The quantum noise is added in the time domain as a Wigner distribution with zero mean value and half a photon standard deviation. The result is shown in Fig. 5 (b), the coherence degree is in effect one over the complete span of frequencies.

Experimentally, we assessed the quality of the SC spectrum by measuring the beat notes between different portions of the broadened comb with a set of continuous wave (CW) lasers. The measurements are carried out by filtering portions of the octave spanning frequency comb. The center region of the input and broadened spectrum was filtered at 1550 nm using a fiber-based narrow filter. The spectrum was also filtered in free space at the 1μm and 2μm regions using a band-pass and edge filter, respectively. Afterwards, each portion of the spectrum was beaten with three different narrow-linewidth lasers at the 1064 nm, 1542 nm and 2006 nm wavelengths. The measurements were performed with two different detectors, an InGaAs photoreceiver with transimpedance gain for the short wavelengths and an extended InGaAs photodetector for longer wavelengths. The photo-detected beat notes were recorded using an electric spectrum analyzer and are shown in Figure 5 (c). The traces shown in the lower row were measured over a span of 255 MHz with a resolution bandwidth (RBW) of 100 kHz. The strongest beat notes at 250 MHz correspond to the repetition rate of the input pulse. The additional two peaks correspond to the beating between the CW laser and the two closest comb lines generated upon broadening. The fact that three clear peaks appear in the RF spectrum indicate that the comb structure is preserved after nonlinear broadening [9, 18]. The upper section of Fig 5 (c) shows a zoom of these beat-notes at a RBW = 10 kHz, an important feature is that the signal to noise ratio is lower at the 1μm and 2μm regions because of the responsivity of the photodectors. However, the radio frequency beat notes at the different regions of the spectrum maintained a narrow-linewidth.

To understand the spectral evolution of the SC, we carried out a set of measurements where the power of the input pulse is varied using a series of optical density filters. Based on the coupling losses measured and the pulse characteristics, we estimated the energy of the in-coupled pulses for each measurement. The measurements are presented in Figure 5 (e), these experimental results are in good qualitative agreement with the simulations using similar energy levels (see Fig. 5 (d)). The broadening occurs at low power levels meaning that a short propagation distance is just enough to perform the broadening when using higher energy pulses. The pulse enters the optical wave breaking regime at around 24 pJ, where the shoulders at the edges of the spectrum akin to the OWB phenomena start to develop [7, 31]. As the input power increases, new

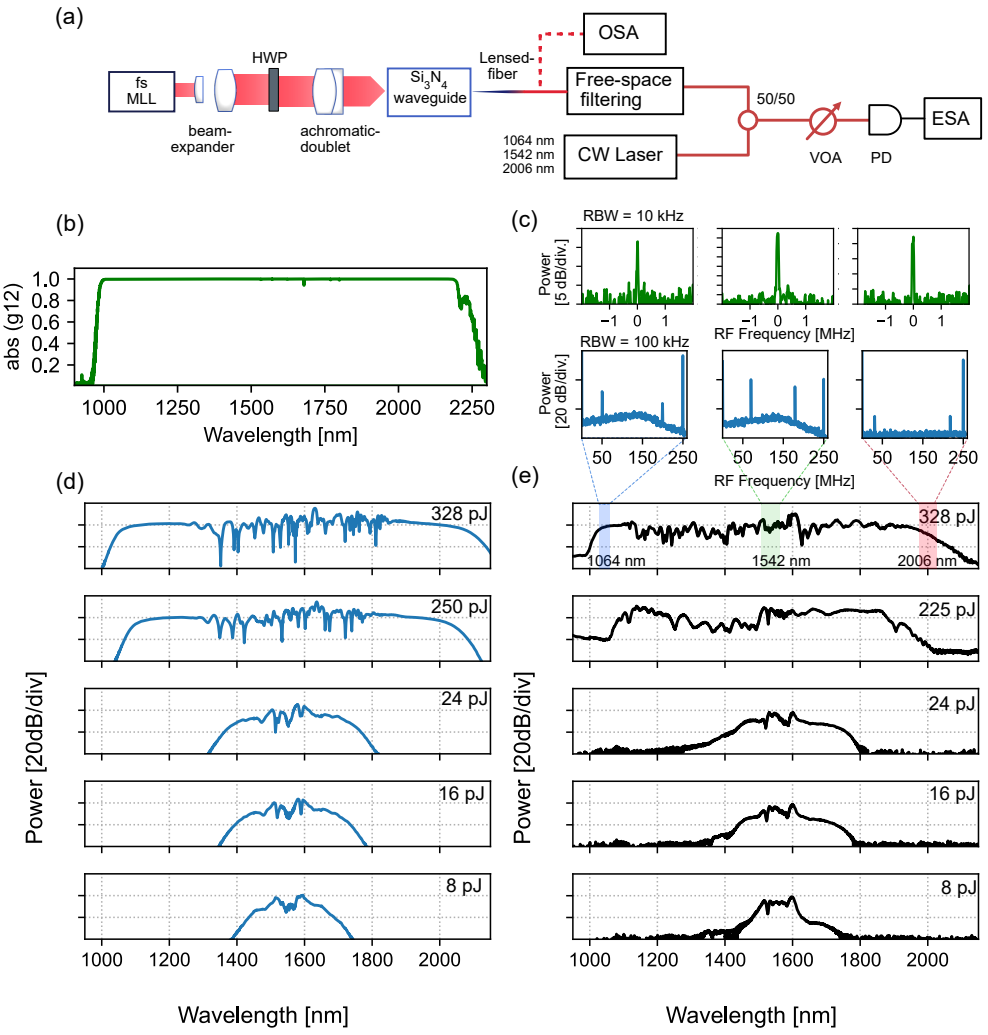

Fig. 5. Supercontinuum generation in a Si_3N_4 ANDi waveguide using femtosecond pump pulses. (a) Experimental setup. MLL: mode-locked laser, HWP: half-wave plate, VOA: variable optical attenuator, PD: photo-detector, ESA: electrical spectrum analyzer. (b) Simulated first order degree of coherence. (c) Measured beat notes resulting of the beating of the filtered SC generated and different CW lasers. (d) Simulated spectra as a function of the injected power. (e) Measured output spectrum using different energies for the input pulses.

frequency components are created as a consequence of the four-wave mixing process related to the wave breaking. The spectral flattening is mostly due to the linearization of the chirp and as a consequence it reshapes into a square spectrum upon propagation. The OWB has occurred after approximately 250 pJ when no more frequency components are created. At the highest input power, the spectrum shows a slight asymmetry due to the stronger dispersion at longer wavelengths (see Fig. 1 (b)) which in turn diminishes the broadening. The spectral output does not show strong intensity variations across the octave bandwidth. However, it exhibits a complex structure as a consequence of the complex shape of the initial pulse [56].

5. Conclusion

In summary, we have designed a three-spiral silicon nitride waveguide that exhibits low and flat dispersion in the all normal dispersion region. The achieved ultra-low losses and long length enable coherent nonlinear broadening of ps pulses at high repetition rate. In this case, the dominant broadening mechanism is self-phase modulation which allows to broad the spectrum near to three times the input pulse bandwidth. These results can be improved by increasing the propagation distance or reducing the dispersion of the waveguide. The phase noise characteristics observed show that the nonlinear processes do not contribute significant additional noise. We have also shown SC generation using pulses with higher energy and femtosecond duration, this in turn allows to access the wave breaking regime to fully observe the SC formation with an octave spanning for the first time in ANDi Si_3N_4 waveguides. The octave spanning spectrum has been filtered and beaten with a set of narrow linewidth lasers. The linewidth of the beat notes imply that the comb structure is maintained across the broadened output. In both cases, the experimental results are in agreement with numerical simulations. These experiments highlight the potential of using ANDi waveguides for stable broadening using picosecond pulses with high repetition rate. The combination of spectral flatness and low noise spectrum enables the on-chip implementation of a variety of applications that already exploit the benefits of nonlinear broadening in the normal dispersion region using dispersion-engineered fibers.

Funding. This project is financially supported by the Swedish Foundation for Strategic Research (FID16-0011), the Swedish Research Council (VR-2020-00453) and the European Research Council (GA 771410 DarkComb).

Acknowledgements. The Si_3N_4 devices were fabricated at Myfab Chalmers.

Disclosures. The authors declare no conflict of interest.

Data availability. The raw data of the measurement results within this work is accessible in [57].

References

1. J. Pfeifle, V. Brasch, M. Lauermann, Y. Yu, D. Wegner, T. Herr, K. Hartinger, P. Schindler, J. Li, D. Hillerkuss, R. Schmogrow, C. Weimann, R. Holzwarth, W. Freude, J. Leuthold, T. J. Kippenberg, and C. Koos, "Coherent terabit communications with microresonator Kerr frequency combs," Nat. photonics **8**, 375–380 (2014).
2. A. Fülöp, M. Mazur, A. Lorences-Riesgo, Ó. B. Helgason, P.-H. Wang, Y. Xuan, D. E. Leaird, M. Qi, P. A. Andrekson, A. M. Weiner, and V. Torres-Company, "High-order coherent communications using mode-locked dark-pulse Kerr combs from microresonators," Nat. communications **9**, 1–8 (2018).
3. S. A. Diddams, M. Kirchner, T. Fortier, D. Braje, A. Weiner, and L. Hollberg, "Improved signal-to-noise ratio of 10 GHz microwave signals generated with a mode-filtered femtosecond laser frequency comb," Opt. Express **17**, 3331–3340 (2009).
4. V. Torres-Company and A. M. Weiner, "Optical frequency comb technology for ultra-broadband radio-frequency photonics," Laser & Photonics Rev. **8**, 368–393 (2014).
5. T. Ideguchi, S. Holzner, B. Bernhardt, G. Guelachvili, N. Picqué, and T. W. Hänsch, "Coherent Raman spectro-imaging with laser frequency combs," Nature **502**, 355–358 (2013).
6. Y. Silberberg, "Combs for molecules," Nature **502**, 307–308 (2013).
7. R. Wu, V. Torres-Company, D. E. Leaird, and A. M. Weiner, "Supercontinuum-based 10-GHz flat-topped optical frequency comb generation," Opt. express **21**, 6045–6052 (2013).
8. N. Singh, D. Vermulen, A. Ruocco, N. Li, E. Ippen, F. X. Kärtner, and M. R. Watts, "Supercontinuum generation in varying dispersion and birefringent silicon waveguide," Opt. express **27**, 31698–31712 (2019).
9. B. Kuyken, T. Ideguchi, S. Holzner, M. Yan, T. W. Hänsch, J. Van Campenhout, P. Verheyen, S. Coen, F. Leo, R. Baets, G. Roelkens, and N. Picqué, "An octave-spanning mid-infrared frequency comb generated in a silicon nanophotonic wire waveguide," Nat. communications **6**, 1–6 (2015).
10. R. Halir, Y. Okawachi, J. Levy, M. Foster, M. Lipson, and A. Gaeta, "Ultrabroadband supercontinuum generation in a CMOS-compatible platform," Opt. letters **37**, 1685–1687 (2012).
11. A. R. Johnson, A. S. Mayer, A. Klenner, K. Luke, E. S. Lamb, M. R. E. Lamont, C. Joshi, Y. Okawachi, F. W. Wise, M. Lipson, U. Keller, and A. L. Gaeta, "Octave-spanning coherent supercontinuum generation in a silicon nitride waveguide," Opt. letters **40**, 5117–5120 (2015).
12. H. Hu, F. Da Ros, M. Pu, F. Ye, K. Ingerslev, E. P. da Silva, M. Nooruzzaman, Y. Amma, Y. Sasaki, T. Mizuno, Y. Miyamoto, L. Ottaviano, E. Semenova, P. Guan, D. Zibar, M. Galili, K. Yvind, T. Morioka, and L. K. Oxenløwe,

"Single-source chip-based frequency comb enabling extreme parallel data transmission," Nat. Photonics **12**, 469–473 (2018).
13. C. Phillips, C. Langrock, J. Pelc, M. Fejer, J. Jiang, M. E. Fermann, and I. Hartl, "Supercontinuum generation in quasi-phase-matched $LiNbO_3$ waveguide pumped by a Tm-doped fiber laser system," Opt. letters **36**, 3912–3914 (2011).
14. J. P. Epping, T. Hellwig, M. Hoekman, R. Mateman, A. Leinse, R. G. Heideman, A. van Rees, P. J. van der Slot, C. J. Lee, C. Fallnich, and K.-J. Boller, "On-chip visible-to-infrared supercontinuum generation with more than 495 THz spectral bandwidth," Opt. express **23**, 19596–19604 (2015).
15. H. Zhao, B. Kuyken, S. Clemmen, F. Leo, A. Subramanian, A. Dhakal, P. Helin, S. Severi, E. Brainis, G. Roelkens, and R. Baets, "Visible-to-near-infrared octave spanning supercontinuum generation in a silicon nitride waveguide," Opt. letters **40**, 2177–2180 (2015).
16. X. Liu, M. Pu, B. Zhou, C. J. Krückel, A. Fülöp, V. Torres-Company, and M. Bache, "Octave-spanning supercontinuum generation in a silicon-rich nitride waveguide," Opt. letters **41**, 2719–2722 (2016).
17. J. M. Dudley and S. Coen, "Coherence properties of supercontinuum spectra generated in photonic crystal and tapered optical fibers," Opt. letters **27**, 1180–1182 (2002).
18. H. Guo, C. Herkommer, A. Billat, D. Grassani, C. Zhang, M. H. Pfeiffer, W. Weng, C.-S. Bres, and T. J. Kippenberg, "Mid-infrared frequency comb via coherent dispersive wave generation in silicon nitride nanophotonic waveguides," Nat. Photonics **12**, 330–335 (2018).
19. K. Tamura, H. Kuhota, and M. Nakazawa, "Fundamentals of stable continuum generation at high repetition rates," IEEE J. Quantum Electron. **36**, 773–779 (2000).
20. R. Oliver, Y. Okawachi, X. Ji, A. R. Johnson, A. Klenner, M. Lipson, and A. L. Gaeta, "Soliton-effect compression of picosecond pulses on a photonic chip," Opt. Lett. **46**, 4706–4709 (2021).
21. Y. Takushima, F. Futami, and K. Kikuchi, "Generation of over 140-nm-wide super-continuum from a normal dispersion fiber by using a mode-locked semiconductor laser source," IEEE Photonics Technol. Lett. **10**, 1560–1562 (1998).
22. C.-B. Huang, S.-G. Park, D. E. Leaird, and A. M. Weiner, "Nonlinearly broadened phase-modulated continuous-wave laser frequency combs characterized using DPSK decoding," Opt. express **16**, 2520–2527 (2008).
23. B. P.-P. Kuo, E. Myslivets, N. Alic, and S. Radic, "Wavelength multicasting via frequency comb generation in a bandwidth-enhanced fiber optical parametric mixer," J. Light. Technol. **29**, 3515–3522 (2011).
24. D. R. Carlson, D. D. Hickstein, W. Zhang, A. J. Metcalf, F. Quinlan, S. A. Diddams, and S. B. Papp, "Ultrafast electro-optic light with subcycle control," Science **361**, 1358–1363 (2018).
25. E. S. Lamb, D. R. Carlson, D. D. Hickstein, J. R. Stone, S. A. Diddams, and S. B. Papp, "Optical-frequency measurements with a Kerr microcomb and photonic-chip supercontinuum," Phys. Rev. Appl. **9**, 024030 (2018).
26. X. Ji, X. Yao, Y. Gan, A. Mohanty, M. A. Tadayon, C. P. Hendon, and M. Lipson, "On-chip tunable photonic delay line," APL Photonics **4**, 090803 (2019).
27. J. Liu, G. Huang, R. N. Wang, J. He, A. S. Raja, T. Liu, N. J. Engelsen, and T. J. Kippenberg, "High-yield, wafer-scale fabrication of ultralow-loss, dispersion-engineered silicon nitride photonic circuits," Nat. communications **12**, 1–9 (2021).
28. Z. Ye, P. Zhao, K. Twayana, M. Karlsson, P. A. Andrekson, and V. Torres-Company, "Ultralow-loss meter-long dispersion-engineered silicon nitride waveguides," in *CLEO: Science and Innovations,* (Optical Society of America, 2021), pp. SF1C–5.
29. S. Christensen, Z. Ye, M. Bache, and V. Torres-Company, "Octave-spanning frequency comb generation in all-normal-dispersion silicon-rich silicon nitride waveguide," in *CLEO: Science and Innovations,* (Optical Society of America, 2020), pp. STu3H–7.
30. E. Tagkoudi, C. G. Amiot, G. Genty, and C.-S. Brès, "Extreme polarization-dependent supercontinuum generation in an uncladded silicon nitride waveguide," Opt. Express **29**, 21348–21357 (2021).
31. C. Finot, B. Kibler, L. Provost, and S. Wabnitz, "Beneficial impact of wave-breaking for coherent continuum formation in normally dispersive nonlinear fibers," JOSA B **25**, 1938–1948 (2008).
32. L. E. Hooper, P. J. Mosley, A. C. Muir, W. J. Wadsworth, and J. C. Knight, "Coherent supercontinuum generation in photonic crystal fiber with all-normal group velocity dispersion," Opt. express **19**, 4902–4907 (2011).
33. A. M. Heidt, J. S. Feehan, J. H. Price, and T. Feurer, "Limits of coherent supercontinuum generation in normal dispersion fibers," JOSA B **34**, 764–775 (2017).
34. A. J. Metcalf, C. D. Fredrick, R. C. Terrien, S. B. Papp, and S. A. Diddams, "30 GHz electro-optic frequency comb spanning 300 THz in the near infrared and visible," Opt. Lett. **44**, 2673–2676 (2019).
35. Z. Ye, K. Twayana, P. A. Andrekson, and V. Torres-Company, "High-Q Si_3N_4 microresonators based on a subtractive processing for Kerr nonlinear optics," Opt. express **27**, 35719–35727 (2019).
36. Z. Ye, P. Zhao, K. Twayana, M. Karlsson, V. Torres-Company, and P. A. Andrekson, "Overcoming the quantum limit of optical amplification in monolithic waveguides," Sci. advances **7**, eabi8150 (2021).
37. Z. Ye, F. Lei, K. Twayana, M. Girardi, P. A. Andrekson, and V. Torres-Company, "Integrated, ultra-compact high-q silicon nitride microresonators for low-repetition-rate soliton microcombs," Laser & Photonics Rev. **n/a**, 2100147 (2021).
38. K. Ikeda, R. E. Saperstein, N. Alic, and Y. Fainman, "Thermal and Kerr nonlinear properties of plasma-deposited silicon nitride/silicon dioxide waveguides," Opt. express **16**, 12987–12994 (2008).

39. K. Twayana, Z. Ye, Ó. B. Helgason, K. Vijayan, M. Karlsson, and V. Torres-Company, "Frequency-comb-calibrated swept-wavelength interferometry," Opt. Express **29**, 24363–24372 (2021).
40. Z. Ye, "Ultralow-loss silicon nitride waveguides for nonlinear optics," Ph.D. thesis, Chalmers Tekniska Hogskola (Sweden) (2021).
41. A. J. Metcalf, V. Torres-Company, D. E. Leaird, and A. M. Weiner, "High-power broadly tunable electrooptic frequency comb generator," IEEE J. Sel. Top. Quantum Electron. **19**, 231–236 (2013).
42. T. Yamamoto, T. Komukai, K. Suzuki, and A. Takada, "Multicarrier light source with flattened spectrum using phase modulators and dispersion medium," J. lightwave technology **27**, 4297–4305 (2009).
43. V. Durán, S. Tainta, and V. Torres-Company, "Ultrafast electrooptic dual-comb interferometry," Opt. Express **23**, 30557–30569 (2015).
44. K. Kashiwagi, H. Ishizu, Y. Kodama, S. Choi, and T. Kurokawa, "Highly precise optical pulse synthesis for flat spectrum supercontinuum generation with wide mode spacing," in *36th European Conference and Exhibition on Optical Communication,* (IEEE, 2010), pp. 1–3.
45. X. Yang, D. J. Richardson, and P. Petropoulos, "Nonlinear generation of ultra-flat broadened spectrum based on adaptive pulse shaping," J. lightwave technology **30**, 1971–1977 (2012).
46. A. M. Weiner, "Ultrafast optical pulse shaping: A tutorial review," Opt. Commun. **284**, 3669–3692 (2011).
47. J. Travers, M. Frosz, and J. Dudley, "Nonlinear fibre optics overview," Supercontinuum Gener. Opt. Fibers p. 32 (2010).
48. G. P. Agrawal, "Nonlinear fiber optics," in *Nonlinear Science at the Dawn of the 21st Century,* (Springer, 2000), pp. 195–211.
49. A. Ishizawa, T. Nishikawa, A. Mizutori, H. Takara, A. Takada, T. Sogawa, and M. Koga, "Phase-noise characteristics of a 25-GHz-spaced optical frequency comb based on a phase-and intensity-modulated laser," Opt. express **21**, 29186–29194 (2013).
50. S. Xiao, L. Hollberg, N. R. Newbury, and S. A. Diddams, "Toward a low-jitter 10 GHz pulsed source with an optical frequency comb generator," Opt. express **16**, 8498–8508 (2008).
51. K. Kikuchi, "Characterization of semiconductor-laser phase noise and estimation of bit-error rate performance with low-speed offline digital coherent receivers," Opt. Express **20**, 5291–5302 (2012).
52. T. Duthel, G. Clarici, C. R. Fludger, J. C. Geyer, C. Schulien, and S. Wiese, "Laser linewidth estimation by means of coherent detection," IEEE Photonics Technol. Lett. **21**, 1568–1570 (2009).
53. R. Maher and B. Thomsen, "Dynamic linewidth measurement technique using digital intradyne coherent receivers," Opt. express **19**, B313–B322 (2011).
54. J. Laegsgaard, "Mode profile dispersion in the generalized nonlinear Schrödinger equation," Opt. express **15**, 16110–16123 (2007).
55. X. Gu, M. Kimmel, A. P. Shreenath, R. Trebino, J. M. Dudley, S. Coen, and R. S. Windeler, "Experimental studies of the coherence of microstructure-fiber supercontinuum," Opt. Express **11**, 2697–2703 (2003).
56. A. Rampur, D.-M. Spangenberg, G. Stępniewski, D. Dobrakowski, K. Tarnowski, K. Stefańska, A. Paździor, P. Mergo, T. Martynkien, T. Feurer, M. Klimczak, and A. M. Heidt, "Temporal fine structure of all-normal dispersion fiber supercontinuum pulses caused by non-ideal pump pulse shapes," Opt. express **28**, 16579–16593 (2020).
57. I. Rebolledo-Salgado, "Raw data for: Coherent supercontinuum generation in all-normal dispersion Si3N4 waveguides," [Data set], Zenodo: Version 1, 16 February 2022 https://doi.org/10.5281/zenodo.6109891.